TheoDORE: a Toolbox for a Detailed and Automated Analysis of Electronic Excited State Computations

F. Plasser[1, a)]
Department of Chemistry, Loughborough University, Loughborough, LE11 3TU, United Kingdom

(Dated: 19 December 2019)

The advent of ever more powerful excited-state electronic structure methods has lead to a tremendous increase in the predictive power of computation but it has also rendered the analysis of these computations more and more challenging and time-consuming. TheoDORE tackles this problem through providing tools for post-processing excited-state computations, which automate repetitive tasks and provide rigorous and reproducible descriptors. Interfaces are available for ten different quantum chemistry codes and a range of excited-state methods implemented therein. This article provides an overview of three popular functionalities within TheoDORE, a fragment-based analysis for assigning state character, the computation of exciton sizes for measuring charge transfer, and the natural transition orbitals used not only for visualisation but also for quantifying multiconfigurational character. Using the examples of an organic push-pull chromophore and a transition metal complex, it is shown how these tools can be used for a rigorous and automated assignment of excited-state character. In the case of a conjugated polymer, we venture beyond the limits of the traditional molecular orbital picture to uncover spatial correlation effects using electron-hole correlation plots and conditional densities.

I. INTRODUCTION

Excited-state electronic structure theory has become increasingly powerful over the last decade thanks not only to increasing computer power but, crucially, due to an immense effort in developing new electronic structure methods.[1–5] Nowadays it is possible to perform excited-state computations on large molecular systems possessing complex electronic structure properties, and it is common to perform statistical sampling or run dynamics using on-the-fly ab initio computations. The analysis of these computations can be challenging not only due to the sheer quantity of data produced but also because new qualitative physics emerges for larger molecular systems. Furthermore, the assignment of wavefunction character based on a visual inspection of orbitals is inevitably subject to personal bias. Therefore, a considerable effort has been devoted to the development of methods for analysing electronic structure computations with the aims of automatising excited-state analysis, making it reproducible, and revealing phenomena that are hidden in the standard molecular orbital (MO) picture. These methods encompass visualisation techniques[6–8] while also a number quantitative descriptors have been designed measuring charge-transfer (CT),[9–13] double excitation character,[8,14–16] and entanglement.[17–20] A particular effort has been devoted to the task of visualising excited-state correlations using correlation plots[21–26] and conditional densities.[27]

The TheoDORE toolbox[28] has been designed with the goal of providing rigorous and detailed excited-state analysis methods in a lightweight and modular framework that is amenable to a variety of electronic structure methods and codes. At the moment interfaces to ten quantum chemistry codes exist encompassing Columbus,[29] OpenMolcas,[30] Q-Chem,[31] ADF,[32] DFTB+,[33] Firefly,[34] Gaussian,[35] Orca,[36] Terachem,[37] and Turbomole,[38] and we will use three of these (Turbomole, Q-Chem, and Orca) in the present work. The analysis is applicable to computations performed with time-dependent density functional theory (TDDFT), coupled cluster, propagator methods as well as with various multireference approaches. TheoDORE provides a set of tools for automating repetitive tasks and generating well-defined data while also allowing to venture into physics beyond the MO picture. Using a fragment-based analysis scheme it is possible to assign the character of several important classes of excited states in a completely automated fashion and the methods have been applied, e.g., to measure delocalisation and CT in interacting DNA bases,[39,40] to quantify how substitution affects the CT character of excited states in donor-acceptor systems,[41] and to assign excited-state character in transition metal complexes.[42,43] More strikingly, the implemented analysis methods allow to understand correlation effects, which are not apparent at all in the standard MO picture with two prominent examples being excitonic correlation in conjugated polymers[44] and the ionic and covalent states in alternating hydrocarbons.[27]

The purpose of this work is to highlight some of the prominent features implemented and to give a compact introduction to new users of the code while a more comprehensive discussion of the available functionalities and the more technical details is given in the literature.[8,25,44] We will focus on three methods, as summarised in Sec. II, a fragment based analysis of the correlated electron-hole pair,[25] the computation of an approximate exciton size,[10,44] and the application of the natural transition orbitals (NTO) decomposition[7,8] for visualising excited states and quantifying their multiconfigurational character.[19] Three exemplary applications are given in Sec. III. First, we show how the excited state character – locally excited vs CT – can be assigned automatically in a push-pull system. We then proceed and apply the same philosophy to an iridium complex and decompose its singlet and triplet states into metal-to-ligand CT (MLCT), ligand-to-ligand CT

[a)]Electronic mail: f.plasser@lboro.ac.uk; https://fplasser.sci-public.lboro.ac.uk

(LLCT), and ligand centred (LC) contributions. Third, exciton correlation occurring in a ladder polymer is illustrated using abstract matrix plots[44] along with a newly developed real-space representation of conditional densities.[27] The more technical details are given in Sec. IV providing an overview of the structure of the code, the computational details, and a step-by-step instruction for performing the analyses and creating the graphics shown here.

II. THEORY

Within this section the theory immediately relevant to this paper is reviewed while more extensive discussions are available in the literature.[8,10,45] The discussion is started with a fragment-based excited state analysis, which is at the centre of this work. Next the computation of an exciton size, which can be defined independently of any fragment definition, is explained. The section is concluded by the discussion of natural transition orbitals as a tool for visualising excited-states as well as for monitoring multiconfigurational character, and a crucial relation between the fragment-based and NTO analyses is shown.

A. Fragment-based excited-state analysis within a correlated electron-hole picture

The main idea behind the fragment-based analysis employed within TheoDORE is illustrated in Fig. 1. First, the system is divided into different fragments. These could be individual chromophores, e.g. interacting DNA bases,[39] units of the same molecule such as the donor and acceptor units in a push-pull system[41] or the ligands in a transition metal complex.[42] In Fig. 1 three such units, labelled 1, 2, and 3, are shown. Within these units, we now proceed to construct different excited states by creating an electron-hole pair. As a first option, exemplified in Fig. 1 (a), the excitation may be entirely localised on an individual fragment. Alternatively, an electron could be transferred between two fragments yielding a charge transfer (CT) state [Fig. 1 (b)]. A third option is the case where local excitations on individual fragments are coupled to yield a delocalised state, denoted a Frenkel exciton. In Fig. 1 (c) such a Frenkel exciton is shown for a case where the dominant contribution is on the central fragment 2 and the other two fragments play a secondary role. A final type of excited state is shown in Fig. 1 (d) representing a linear combination of two CT states going in opposite directions yielding a charge resonance state. The important realisation from Fig. 1 is that it is not generally enough to know the overall distributions of the hole and electron, i.e. the locations of the red and blue dots, but that their dynamic connection as represented by the arrows is also important. To exemplify this observation, we note that cases (c) and (d) appear similar when looking at the independent electron and hole distributions in the sense that both quasi-particles are distributed over several fragments and that no net CT occurs. However, once the arrows in Fig. 1 are taken into account, the situation changes: case (c) is seen to be a tightly bound Frenkel exciton state while (d) is a charge separated state. The physical implication of this is readily seen when the distance of the chromophores is separated: The energy of the Frenkel states stay roughly the same while the energy of the charge resonance states increases as $1/R$ (where R is the intermolecular separation).[10,25]

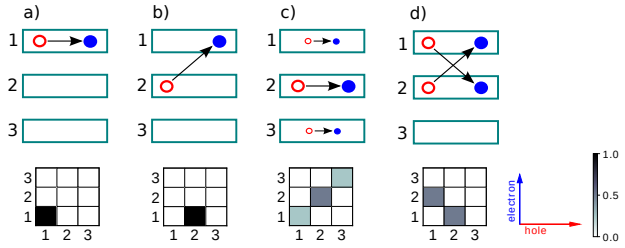

FIG. 1. Different types of excited states distributed over three coupled fragments: (a) local excitation on fragment 1, (b) charge transfer from 2 to 1, (c) delocalised Frenkel state, (d) charge resonance state. Top: graphical representation of the distribution of the hole (red) and electron (blue) over the fragments; bottom: analysis via electron-hole correlation plots.

Motivated by the above discussion, we have devised an excited-state analysis scheme based around the concept of a correlated electron-hole pair.[8,10,25,45] In a first step, an effective wavefunction for the electron-hole pair has to be defined. For this purpose, we consider the one-electron transition density matrix (1TDM) between the ground and excited states, which can be written as the integral

$$\gamma_{0I}(r_h,r_e) = n\int\ldots\int \Psi_0(r_h,r_2,\ldots,r_n)\Psi_I(r_e,r_2,\ldots,r_n)\mathrm{d}r_2\ldots\mathrm{d}r_n \tag{1}$$

where Ψ_0 and Ψ_I are the ground and excited state wavefunctions. The coordinates r_h and r_e represent the hole and electron, which originate from Ψ_0 and Ψ_I, respectively. Using the 1TDM, we can now proceed to decompose the excitation into different local and CT contributions. For this purpose, we compute the charge transfer numbers,[25,46] which can formally be written as the integral

$$\Omega_{AB} = \int_A\int_B |\gamma_{0I}(r_h,r_e)|^2\mathrm{d}r_e\mathrm{d}r_h \tag{2}$$

where the hole is restricted to a fragment A of the system and the electron to fragment B. Practically speaking the integral in Eq. (2) is evaluated using a population analysis scheme leading to straightforward matrix operations and one can either use a formula[8,25] analogous to Mayer's bond order[47] or work with Löwdin orthogonalisation.[43,48]

After the Ω-matrix collecting all Ω_{AB} values is computed, it can be conveniently visualised in a pseudocolor matrix plot, the so-called Ω-plot or electron-hole correlation plot.[44] In the case of three fragments, the Ω matrix is of dimension 3×3 and we show the corresponding Ω-plots in the bottom row of Fig. 1. The origin is in the lower left corner and the hole and electron coordinates extend along the horizontal and vertical axes, respectively. In case (a), the hole and electron are both confined to fragment 1 and we obtain a value of $\Omega_{11}=1$ while

all other elements vanish. This is represented in Fig. 1 (a) by a matrix where only the element on the lower left is coloured. In Fig. 1 (b), the hole is on fragment 2 while the electron is on fragment 1 yielding $\Omega_{21} = 1$ and the corresponding matrix plot is shown at the bottom. In the case of delocalised states several elements of the Ω-matrix possess non-vanishing values where locally excited contributions appear on the main diagonal (going from lower left to upper right) while CT contributions appear off-diagonally. These two cases are represented in Fig. 1 (c) and (d), respectively. Once the charge transfer numbers are computed it is either possible to directly visualise the Ω-plots to see the correlated structure of the exciton[44] or to compress the information into more compact bar graphs[43] as explored below. If larger data sets are of interest one can, of course, skip the visualisation process altogether and directly proceed to a statistical analysis, which is particularly useful when studying an ensemble[39,40] or when performing dynamics simulations.[49,50]

Whereas the Ω-matrices provide a very compact representation of the correlated exciton, this representation may be too abstract in many cases. Therefore, a different representation has been developed,[27] which formally proceeds by modifying Eq. (2) in the sense that only one of the integrations is carried out leaving the one-body function

$$\rho_e^{h:A}(r_e) = \int_A |\gamma_{0I}(r_h, r_e)|^2 \mathrm{d}r_h \,. \tag{3}$$

The function $\rho_e^{h:A}$ is interpreted as the conditional electron density obtained under the constraint that the probe hole is restricted to fragment A. The correlated structure of the exciton can now be visualised by moving the probe hole to different fragments of the system and computing the corresponding conditional electron densities.[27] Note that related ideas have been used for visualising exciton structure in solids[51,52] as well as Fermi holes[53] and spin-correlation in molecules.[54]

B. The exciton size

A downside of the fragment-based analysis scheme is that it requires an a-priori definition of the fragments and that the results obtained may depend on the representation chosen. A possibility of avoiding this ambiguity is by automatising the fragmentation procedure via correlations between the different fragments.[43] However, in other cases it is desirable to avoid the definition of fragments altogether and we have devised an analysis scheme of the exciton wavefunction in real space for this purpose. This allows monitoring of the average separation between the electron and hole, the spatial extent of the individual contributions as well as correlation effects.[10,45,55] However, this requires additional information from the quantum chemistry program that is usually not available to TheoDORE. Therefore, we have directly implemented the methods within the Q-Chem[31] and OpenMolcas[30] packages via TheoDORE's sister project, the wavefunctiona analysis library libwfa.[56] Nonetheless, one property derived from these works can be computed within TheoDORE, the approximate exciton size[44] defined as

$$\tilde{d}_{exc} = \sqrt{\Omega^{-1} \sum_{MN} \Omega_{MN} {d_{MN}}^2} \tag{4}$$

where Ω_{MN} is the charge transfer number computed with respect to two atoms M and N, and d_{MN} is the distance between these atoms. Ω is the normalisation factor defined as the sum over all Ω_{MN} elements. $\tilde{d}_{exc}$ gives the root-mean-square separation of the electron and hole (denoted `RMSeh` in TheoDORE) in a point charge approximation. An exciton size below about 4 Å usually reflects a purely local excitation while higher values are indicative of CT contributions.

C. Natural transition orbitals

A convenient tool for analysing excited state computations is given via the natural transition orbital (NTO) decomposition.[7,25] The NTOs are computed through a singular value decomposition and allow for representing the 1TDM in the following form[8]

$$\gamma_{0I}(r_h, r_e) = \sum_t \sqrt{\lambda_t}\, \psi_t^h(r_h) \psi_t^e(r_e), \tag{5}$$

i.e. as a single sum over orbital pairs where ψ_t^h and ψ_t^e are the NTOs representing the hole and electron and λ_t is the amplitude of the transition. Usually only one or a small number of λ_t values are notably above zero and, thus, the NTO decomposition tends to provide a very compact representation of the excitation. But the utility of the NTO decomposition does not only lie in the pictorial representations it provides but also the singular values themselves contain important physical information by providing a natural measure of the multiconfigurational character of the excited state.[19,25] To measure the multiconfigurational character, we have suggested to count the number of configurations via the NTO participation ratio[19,25] (equivalent to Luzanov's collectivity number[46])

$$\mathrm{PR_{NTO}} = \frac{\left(\sum_t \lambda_t\right)^2}{\sum_t \lambda_i^2}. \tag{6}$$

If a state can be described by a single transition between two NTOs then $\mathrm{PR_{NTO}}$ is equal to 1 while higher values are obtained for multiconfigurational states.

At first sight one would assume that the $\mathrm{PR_{NTO}}$ value, which regards the singular value structure of the 1TDM, and the charge-transfer numbers, which encode spatial information, are independent from each other. However, there is an interesting relation. If we assume that $\mathrm{PR_{NTO}}$ is exactly equal to 1, then it follows that the 1TDM factorises into a single pair of NTOs according to

$$\gamma_{0I}(r_h, r_e) = \psi^h(r_h) \psi^e(r_e) \,. \tag{7}$$

In this case the charge transfer numbers [Eq. (2)] are given as

$$\Omega_{AB} = \int_A \int_B |\psi^h(r_h)\psi^e(r_e)|^2 \mathrm{d}r_e \mathrm{d}r_h = \int_A |\psi^h(r_h)|^2 \mathrm{d}r_h \times \int_B |\psi^e(r_e)|^2 \mathrm{d}r_e = q_A^h q_B^e, \tag{8}$$

i.e., the Ω_{AB} values are already completely determined by the shapes of the individual NTOs; they are simply given as the product of the hole and electron charges (q_A^h, q_B^e) on fragments A and B, respectively. Similarly one finds that under the assumption (7) the conditional electron density

$$\rho_e^{h:A}(r_e) = \int_A |\psi^h(r_h)\psi^e(r_e)|^2 \mathrm{d}r_h = q_A^h \times |\psi^e(r_e)|^2 \qquad (9)$$

is independent of the location of the probe hole A except for the constant factor q_A^h. Thus, we conclude that non-trivial interference effects, requiring an analysis in terms of a correlated electron-hole picture, can only come into play if $\mathrm{PR_{NTO}}$ is significantly larger than 1. Nonetheless, it is the strength of the presented protocol that it works equally well for simple orbital-to-orbital transitions as it does for more complicated excited states and we want to highlight the generality of the presented approach below.

III. EXAMPLE APPLICATIONS

Within this section we want to exemplify applications of TheoDORE using different case studies focussing on the question of how excited state character can be represented in the form of a few well-defined and meaningful numbers. Three problems of increasing complexity are chosen. Firstly, we regard a simple organic push-pull chromophore whose analysis in terms of canonical MOs would also be possible. However, TheoDORE offers the advantage of being automated and of providing quantitative results. Secondly, we study a heteroleptic iridium complex where the assignment of excited-state character becomes significantly more difficult due to non-trivial interactions between states of different character making the utility of the described methods immediately apparent. Finally, we discuss states in a conjugated oligomer. In this system non-trivial electron-hole correlation effects come into play, which would be exceedingly difficult to identify in the canonical MO picture.

A. Quantification of charge-transfer in push-pull systems

A common task encountered when performing excited state computations is to classify excited states according to their character and to specify where the excitations are located or whether charge transfer occurs. These questions can be conveniently addressed with the tools described in Section II A. For the purpose of this work, we present some results on the recently reported[57] push-pull chromophore $\mathrm{ZMSO_2}$M-14TPA (Z-methylsulfonylpropenyltriazolyl-triphenylamine) shown in Fig. 2 (a). In Fig. 2 (b), the excitation energies of the first nine singlet states are shown and their oscillator strengths are given as shading (increasing as white < blue < orange). This representation shows that the brightest state (with an oscillator strength of 0.667) is S_1, located just below 4 eV while several higher energy bright states follow. In a next step, we proceed to classify the excited states in this system. As shown in Fig. 2 (a), the molecule is composed of the electron donor triphenyl amine (TPA, blue) as well as two acceptor groups, first a triazole ring (green) and, second, the Z-methylsulfonylpropenyl group ($\mathrm{ZMSO_2}$, red). We compute the CT numbers [Eq. (2)] with respect to these three fragments and group them into the following four contributions: (i) the local excitation on TPA (Ω_{11}), (ii) CT from TPA to triazole (Ω_{12}), (iii) CT from TPA to $\mathrm{ZMSO_2}$ (Ω_{13}), and (iv) any excitations on triazole and $\mathrm{ZMSO_2}$ ($\Omega_{22}+\Omega_{33}+\Omega_{23}+\Omega_{32}$). In Fig. 2 (c) a bar graph is shown that divides every state according to those four contributions. We find that the bright S_1 state is dominated by local excitations on TPA (blue) but that it also possesses non-negligible TPA→triazole CT character (green). Three states completely localised on TPA follow. The second one of these (S_3), possessing an oscillator strength of 0.240, gives rise to an experimentally observed band at around 300 nm, which is characteristic for TPA-substituted molecules.[57] S_5 follows with enhanced TPA→$\mathrm{ZMSO_2}$ character while S_6 is again localised on TPA. Two states on the triazole and $\mathrm{ZMSO_2}$ units follow. And finally, S_9, is seen to be of mixed character. The NTOs [Eq. (5)] for selected states are plotted in Fig. 2 (d) where the hole is shown on the bottom and the electron at the top. The NTOs support the assignments made earlier: S_1 is located on TPA but possesses important CT contributions; S_2 is entirely TPA-centred; S_7 is delocalised over the triazole and $\mathrm{ZMSO_2}$ units.

In summary, this analysis shows that the excited-state character in a push-pull system can be automatically assigned using the presented protocol. The results are consistent with a manual assignment of state character only that a completely quantitative picture is obtained. Using this data one may now proceed to studying the scientific question of interest, for example one may compare[57] how the excited states are affected by different substitution patterns or solvation.

B. State assignment in transition metal complexes

Transition metal complexes are a particularly interesting application area for the fragment-based analysis discussed here for two reasons. First, the assignment of excited states in transition metal complexes is notoriously challenging and tedious due to the fact that a large number of excited states are involved and that it is difficult to assign the excited-state character directly from the canonical orbitals.[43,58,59] Second, the excited states are usually discussed in a fragment based picture, which is particular amenable to TheoDORE. The states are classified into, e.g., LC, MLCT, or LLCT character, which can be directly identified with different blocks of the Ω-matrix.[42,43]

For the purpose of this work, we regard the bis-phenyltriazole-bipyridyl iridium complex $[\mathrm{Ir(ptz)_2bpy}]^+$.[60,61] The molecular structure of $[\mathrm{Ir(ptz)_2bpy}]^+$ is shown in Fig. 3 (a). To the left the phenyltriazole (ptz) ligands (red) are shown, which act as electron donors. The iridium (yellow) is in the centre. The bipyridyl electron acceptor (blue) is shown to the right. Eight singlet and triplet excited states were computed for this complex at the TDDFT/PBE0 level of

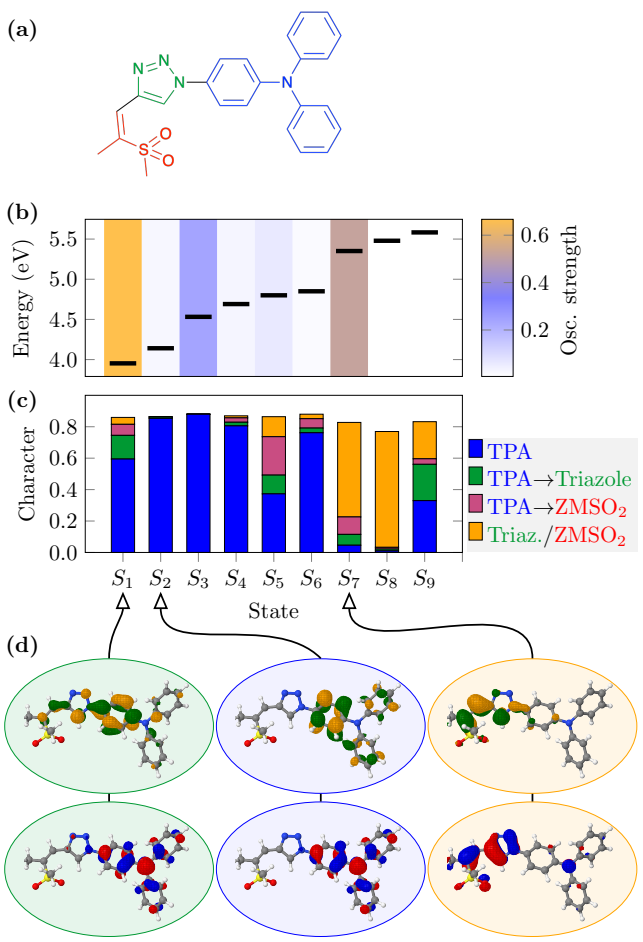

FIG. 2. Fragment-based analysis of excited-states in an organic push-pull system using TheoDORE based on RI-CC2 computations in Turbomole. Molecular structure (a) of the $ZMSO_2$M-14TPA molecule and its decomposition into three fragments – triphenylamine (TPA, blue), triazole (green), Z-methylsulfonylpropenyl ($ZMSO_2$, red); excitation energies and oscillator strengths (b); excited-state character (c) automatically assigned using the CT numbers; and exemplary NTOs (d) for the S_1, S_2, and S_7 states.

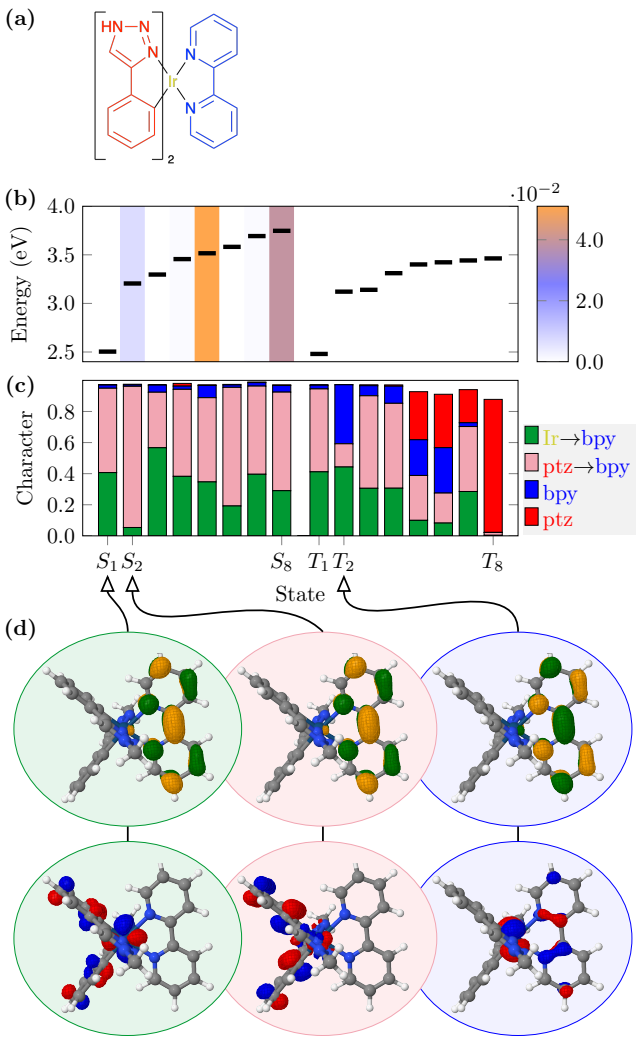

FIG. 3. Fragment-based analysis of excited-states in a transition metal complex using TheoDORE based on TDDFT/PBE0 computations in Q-Chem. Molecular structure (a) of the $[Ir(ptz)_2bpy]^+$ complex and its decomposition into three fragments – bipyridyl (bpy, blue), iridium (yellow), and phenytriazole (ptz, red); excitation energies and oscillator strengths (b); excited-state character (c); and exemplary NTOs (d) for the S_1, S_2, and T_2 states.

theory. Their excitation energies and oscillator strengths are presented in Fig. 3 (b) showing that the S_1 and T_1 energies are both located at around 2.5 eV while all other states are well above 3 eV. S_1 and T_1 possess similar characters showing around half Ir→bpy (green, MLCT) and ptz→bpy (pink, LLCT) character. Interestingly, S_2 and T_2 strongly differ in their characters. S_2 is almost entirely of ptz→bpy (pink) type whereas T_2 possess strong LC contributions on bpy (blue). We can understand this phenomenon in the sense that locally excited singlet states in small chromophores face a strong energetic penalty through exchange repulsion (cf. Ref. 62) and are, therefore, at higher energies. In accordance with this, we find that the first eight singlet states are only composed of CT contributions (green, pink) while enhanced local character (blue, red) comes into play for the triplets. The NTOs for three selected states (S_1, S_2, T_1) are shown in Fig. 3 (d). The dominant electron NTO (top) is always located on bpy; it corresponds the lowest unoccupied MO (LUMO) in the canonical MO picture. The dominant hole NTO (bottom) changes among the states. For S_1 it is delocalised over the ptz units and Ir whereas it is almost completely localised on the ptz units for S_2. For T_2, by contrast, the hole NTO is distributed over Ir and bpy. Thus, the NTOs reflect the same trends as the fragment based analysis only that it is challenging to produce quantitative results from looking at the NTOs alone and this becomes even more difficult when using canonical MOs.

We hope that we could illustrate that the protocol retrieves non-trivial information about the excited states in an automated and well-defined way. The interested reader is referred to Ref. 43 for more information on how the approach can be used to tackle a variety of questions in transition-metal-complex photochemistry.

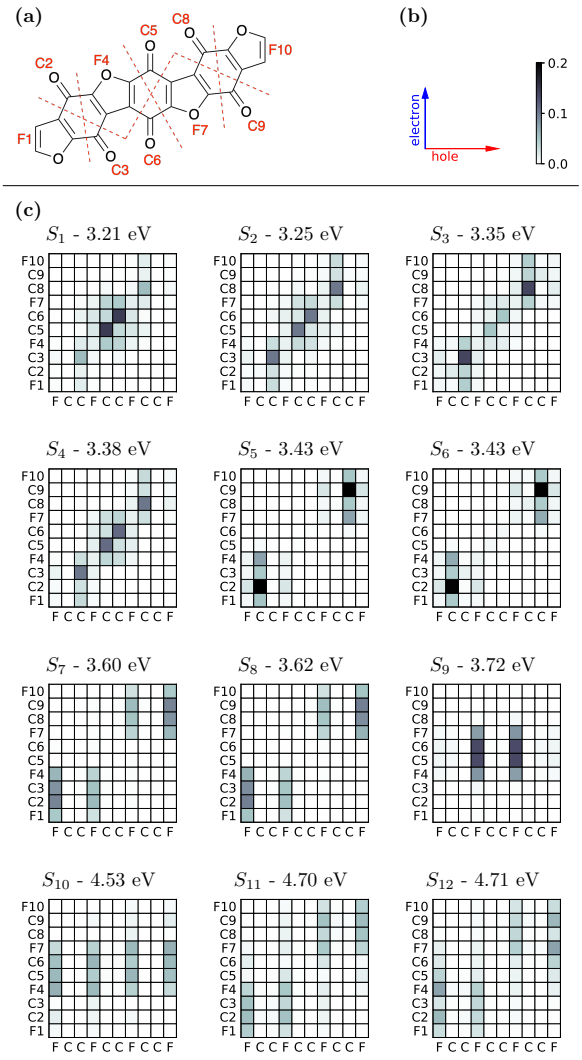

FIG. 4. Analysis of electron-hole correlation considering the conjugated ladder oligomer $(FC)_3F$. Molecular structure (a) and fragment definition considering four furane rings (F1, F4, F7, F10) and six CO fragments (C2, C3, C5, C6, C8, C9); depiction of color scale and coordinate definition (b); electron-hole correlation plots (c).

C. Visualisation of correlation effects in large conjugated systems

In the case of smaller molecules, it is often sufficient to describe an excited state in terms of two involved orbitals, e.g. a HOMO-LUMO transition. However, in larger systems a number of quasi-degenerate orbitals come into play leading to quasi-degenerate electron configurations, which interact to form multiconfigurational excited states. Physically speaking one can interpret states in these systems as deriving from two interacting quasi-particles moving through the system, the electron and the hole,[22,62,63] and specialised methods have been developed to depict their correlated structure.[23,26,44,51]

For the purpose of this work, we study the ladder oligomer shown in Fig. 4 (a).[64,65] This molecule is composed of four furane (F) units bridged by six CO (C) units and we will denote

TABLE I. Excitation energies (ΔE, eV), oscillator strengths (f), NTO participation ratios (PR_{NTO}), approximate exciton size ($\tilde{d}_{exc}$, Å), and type assignment for the first 12 singlet excited states of the conjugated ladder oligomer $(FC)_3F$.

State	ΔE	f	PR_{NTO}	$\tilde{d}_{exc}$	type
S_1	3.21	-	1.92	2.87	$n\pi^*$
S_2	3.25	-	2.85	2.83	$n\pi^*$
S_3	3.35	-	3.06	2.82	$n\pi^*$
S_4	3.38	-	2.93	2.78	$n\pi^*$
S_5	3.42	-	2.06	2.76	$n\pi^*$
S_6	3.43	-	2.20	2.75	$n\pi^*$
S_7	3.60	0.017	1.99	3.32	$\pi\pi^*$
S_8	3.62	-	2.08	3.24	$\pi\pi^*$
S_9	3.72	-	1.04	3.58	$\pi\pi^*$
S_{10}	4.53	0.036	1.39	5.08	$\pi\pi^*$
S_{11}	4.70	0.195	2.40	4.04	$\pi\pi^*$
S_{12}	4.71	-	2.58	4.63	$\pi\pi^*$

it $(FC)_3F$. $(FC)_3F$, derived from hexeneuronic acid, is found in cellulosic pulps where it is a cause for discolouration.[64] While this discolouration is unwanted in cellulose one may ponder whether this strongly absorbing chromophore[64] may ultimately be used as a basis for optoelectronic applications and we will proceed to study its electronic structure here. The excitation energies of the first 12 singlet excited states of this molecule are shown in Table I. The first six excited states are all within a very narrow energy window of 3.21-3.43 eV and are of $n\pi^*$ type. These six states are formed as linear combinations of the $n\pi^*$ transitions originating on the individual CO groups. The remaining six states in Fig. 4 are all of $\pi\pi^*$ nature. The first three states (S_7-S_9) are closely spaced in the energy window 3.60-3.72 eV while the second set set (S_{10}-S_{12}) lies significantly higher at 4.53-4.70 eV. In agreement with Ref. 66 we find that the first bright state (S_7) is at around 3.60 eV only that S_7 as computed here shows a significantly lower oscillator strength when compared to the B3LYP results of Ref. 66. The brightest state shown here is S_{11} located at 4.70 eV.

In order to visualise the pair distribution of electron and hole, we plot the charge transfer numbers Ω_{AB} [Eq. (2)] in the form of a pseudocolor matrix plot in Fig. 4 (c). The employed coordinate system is shown in Fig. 4 (b): The origin is in the lower left corner and the hole and electron coordinates extend along the horizontal and vertical axes, respectively. Any local contributions are on the main diagonal going from lower left to upper right while the other elements refer to CT. The value of the respective Ω_{AB} element is given by a colour scale going from white to black. In general these plots are to be interpreted as indicated in Fig. 1. Inspection of the plots of the six $n\pi^*$ states (S_1-S_6) shows that all the dominant contributions are local CO→CO elements with some diffuse contributions around them. To understand what this means we proceed to a more extended analysis selecting the S_4 state as an example. The overall distributions of the hole and electron for this state are shown in Fig. 5 (a). We find the hole (red) centred around the non-bonding orbitals on oxygen while the electron (blue) resides in the π-system reflecting the $n\pi^*$ nature of this state. In a next step, we want to understand the electron-

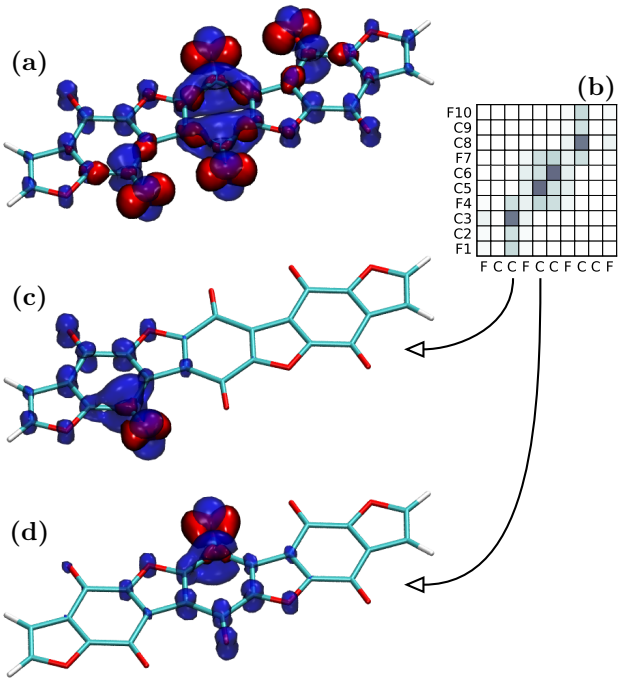

FIG. 5. Detailed analysis of the S_4 state of the conjugated ladder polymer $(FC)_3F$: the overall hole (red) and electron (blue) densities (a); electron-hole correlation plot (b); conditional electron densities computed for the hole localized on carbonyl unit C3 (c) and C5 (d). The surfaces plotted encompass 75% of the total electron densities.

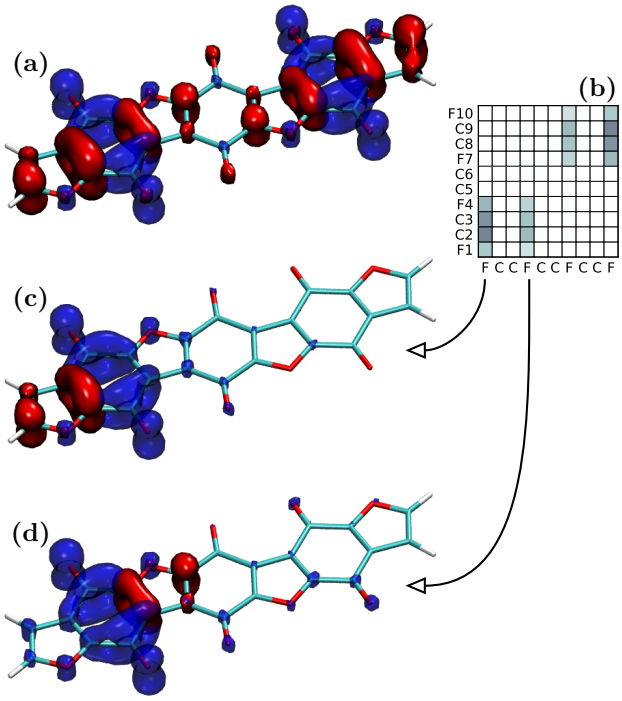

FIG. 6. Analysis of the S_7 state of the conjugated ladder polymer $(FC)_3F$: the overall hole (red) and electron (blue) densities (a); electron-hole correlation plot (b); conditional electron densities computed for the hole localized on furan unit F1 (c) and F4 (d). The surfaces plotted encompass 75% of the total electron densities.

hole correlation plots in more detail. This is achieved via the conditional electron densities [Eq. (3)], which effectively provide real space representations of individual columns of the electron-hole correlation plot. In Fig. 5 (b) we find that there are four columns with significant contributions: C3, C5, C6, and C8. We choose the two symmetry-unique contributions C3 and C5 and compute the corresponding conditional densities. These are shown in Fig. 5 (c) and (d), respectively. The probe hole (red) resides, per construction, only on the respective carbonyl group (C3 or C5). Interestingly, we find that the conditional density is strongly pulled toward the probe hole despite the fact that the total density of the excited electron [Fig. 5 (a), blue] is distributed over a large part of the molecule. There is only some "spillover" to the other CO group on the same ring and almost no contributions going to CO groups on other rings. This illustrates how correlation effects always keep the electron and hole close together, thus, enhancing their dynamic Coulomb attraction (see also Ref. 62). In the Ω-plot Fig. 5 (b) this fact is represented by the fact that the plot is strongly dominated on the diagonal (going from lower left to upper right). From a different viewpoint we may view the CO groups as largely electronically decoupled units. This is also consistent with the fact that all six $n\pi^*$ states are contained in a narrow energy window of only 0.2 eV.

Proceeding to the Ω-plots of the $\pi\pi^*$ states S_7-S_{12} in Fig. 4, we find that all these states possess contributions in the columns labelled "F", i.e., the hole is located on different furan units, while the electron is at the same or adjacent furan and CO units. A detailed discussion of S_7 is presented in Fig. 6 (a) starting with the overall electron and hole densities in panel (a). The hole (red) is distributed in the π-system across the furan units while the electron (blue) resides mostly on the outer CO groups. When the hole is restricted to the F1 [Fig. 6 (c)] or F4 [Fig. 6 (d)] fragments, we find that the electron is confined to the same side of the molecule where also F1 and F4 are located. Interestingly, the shape of the conditional electron density is almost invariant with respect to the choice of fragment (F1 or F4). For symmetry reasons it follows that with the hole located on F7 and F10 the electron would be located on the other side. This shows that the molecule is effectively divided into two halves in the sense that the conditional density is always located on the same half as the probe hole but that it is independent of the probe hole's precise position within that half. This division is reflected in the block-diagonal structure of the Ω-plot in Fig. 6 (b). Proceeding to S_8 one finds that this state is only 0.02 eV above S_7 and its Ω-plot possesses almost the same structure as S_7. This suggests that S_7 and S_8 can be seen as the $+/+$ and $+/-$ combinations composed of largely decoupled local excitations on the two halves of the molecule. The S_9 state has a similar pattern in Fig. 4 only that the excitation is concentrated at the central ring.

To understand the difference between the states S_7-S_9 and

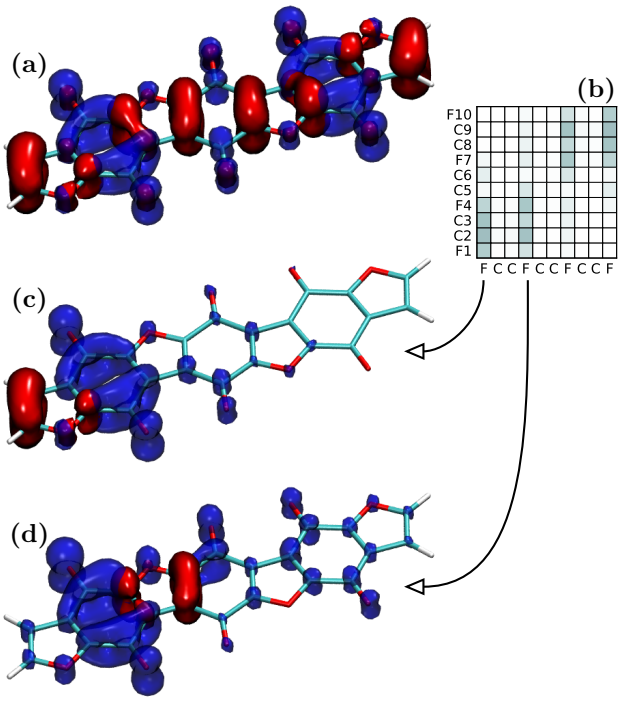

FIG. 7. Detailed analysis of the S_{11} state of the conjugated ladder polymer $(FC)_3F$: the overall hole (red) and electron (blue) densities (a); electron-hole correlation plot (b); conditional electron densities computed for the hole localized on furan unit F1 (c) and F4 (d). The surfaces plotted encompass 75% of the total electron densities.

S_{10}-S_{12}, we proceed to an analysis of the S_{11} state [Fig. 7]. The overall electron and hole densities of S_{11} are shown in Fig. 7 (a) resembling S_7 with the exception that the hole is somewhat more strongly concentrated on the centre. Restricting the hole to F1 [Fig. 7 (c)] gives a very similar shape as obtained for the S_7 state. By contrast, if the probe hole is on F4 [Fig. 7 (d)] we find that the conditional electron density spills over to the other side of the molecule much more strongly than in the case of S_7 meaning that it is no longer confined to the left half of the molecule. More generally, we can thus understand the difference between the first three states (S_7-S_9) and the last three states (S_{10}-S_{12}) in the sense that the former are more tightly bound than the latter. This is also apparent by the fact that the Ω-plots are more diffuse for S_{10}-S_{12}. To have a more quantitative measure, we use the approximate exciton size $\tilde{d}_{exc}$ as presented in Tab. I. This measure shows S_7-S_9 to be more tightly bound with exciton sizes well below 4 Å while they are above this value for S_{10}-S_{12}.

Finally, we want to discuss the PR_{NTO} measure also given in Tab. I. PR_{NTO} measures the multiconfigurational character of the excited-state by counting the number of non-vanishing singular values of the 1TDM. PR_{NTO} values well above 1 are found for all states except S_9 and S_{10} illustrating that most of these states do indeed possess non-trivial multiconfigurational character and, as explained at the bottom of Section II C, this also means that the CT-number analysis can provide information that would not be retained with an independent analysis of electron and hole densities. Before concluding this section, we can proceed further and relate the PR_{NTO} value to the block structure of the Ω-plots. First, it can be realised that a block-diagonal 1TDM will have at least one non-vanishing singular value per block. Second, we can attempt to choose a fragmentation scheme that preserves this block structure in the Ω-matrix. As a consequence, one can posit that the number of blocks in the Ω-plot is reflected by the PR_{NTO} value. This is indeed the case for the states shown here. The states S_5-S_8 all show Ω-plots of two independent blocks and indeed their PR_{NTO} values are very close to 2. The next state, S_9, is represented by just one central block in Fig. 4 and, indeed, its PR_{NTO} value is only 1.04. S_{10} possesses a rectangular plot with sufficiently little structure to allow for a low PR_{NTO} value of 1.39. By contrast the states S_2, S_3, S_4, S_{11}, and S_{12} all possess Ω-matrices with more structure leading to higher PR_{NTO} values. This illustrates the relations[19] between the more abstract PR_{NTO} value and actual spatial correlation effects. Finally, we want to point out that it is also possible to view PR_{NTO} as an effective matrix rank[46] and use this as a basis for the argument, i.e. two independent blocks will always contain at least two linearly independent columns and thus lead to a rank of at least 2.

An overall comparison of the low energy energy states of $(FQ)_3F$ to previous similar studies on oligo-phenylene-vinylene (OPV)[44,67] and oligothiophene (OT)[27] suggests a different behaviour between the former and the latter two. OPV and OT both possess a bright, energetically well-separated, and loosely bound S_1 state whereas $(FQ)_3F$ possesses a number of dark, closely spaced and strongly bound low energy states. This suggests a different photophysical behaviour and it is reasonable to speculate that the CO groups act as dark trapping sites meaning that exciton mobility and luminescence will be lower in $(FQ)_3F$ when compared to OPV or OT. Nonetheless, these properties may be altered through chemical substitution and $(FQ)_3F$ may act as a starting point in the design of new conjugated systems.

IV. TECHNICAL DETAILS

Before concluding, we want to mention the relevant technical details. We will commence by discussing the overall structure of the TheoDORE code and proceed by listing the computational details. Finally, we want to elaborate on a step-by-step instruction to allow the interested reader to create related graphics themselves.

A. Structure of the TheoDORE code

TheoDORE is designed with the aim of providing a lightweight yet versatile program package. The code is written in python and encompasses about 12000 lines. It is available open-source.[28] Extensive use is made of external libraries and programs for various tasks. The code is interfaced to the following five external libraries: NumPy[68] for matrix operations, matplotlib[69] for creating Ω-plots and di-

verse graphs, openbabel[70] for handling of molecular structures, cclib[71] for interfaces to different quantum chemical programs, and orbkit[72] for evaluating orbitals and densities on a grid. TheoDORE possesses no graphical user interface but various programs are integrated into the workflow. Avogadro[73] can be used for the fragment definition process. The graphical output of NTOs and various other types of orbitals is automatated via scripts for the Jmol[74] program. TheoDORE also possesses a utility for automatically creating plots of the conditional electron densities or any other cube files of interest via a VMD[75] script. Alternatively, cube files produced via TheoDORE plots can be easily visualised in PyMOL[76] when using the qc_pymol toolkit.[77] Finally, some output graphics can be generated via LaTeX/TikZ.

TheoDORE is designed as to require only minimal information from the quantum chemistry program and to require only minimal computational effort. The fragment-based analysis proceeds using only two piecees of information: (i) the MO-coefficients along with the information where the MOs are located and (ii) the response vectors. Crucially, it is not necessary to provide the AO overlap matrix as it is reconstructed internally from the MO-coeffients.[25,43] The MO-coefficients and response vectors are readily available from most quantum chemistry codes as they are the same information that is also used for a traditional analysis of excited-state character. Therefore, new interfaces can be created easily. The operations shown in Eqs (2-5) can be readily written as matrix multiplications, which are implemented via the NumPy[68] library. No grid-based numerical integration or other computationally expensive tasks are employed and, therefore, the TheoDORE analysis usually only takes a small fraction of the time of the preceding ab initio computation.

B. Computational details

The geometry of $ZMSO_2M$-14TPA was taken from Ref. 57 and excited-state computations were performed using the approximate coupled cluster method RI-CC2,[78] as implemented in Turbomole V7.2,[38] in connection with the def2-SV(P) basis set.[79] The geometry optimisation and computation of vertical excitation energies of $[Ir(ptz)_2bpy]^+$ was performed using (TD)DFT in the Tamm-Dancoff approximation[80] at the PBE0/def2-SV(P)[81] level within a development version of Q-Chem 5.2.[31] $(FQ)_3F$ was optimised at the B3LYP/def2-SV(P) level.[82,83] The excited states were computed using CAM-B3LYP/def2-SVP[84] employing the RIJCOSX[85] approximation within Orca 4.1.2.[36] The computations were post-processed using a developmental version of TheoDORE 2,[8,25,28] and the full functionality described here will be made available through TheoDORE 2.1. The underlying research data (molecular geometries, input/output files, data underlying the figures) is provided via a separate repository.[86]

C. Step-by-step instruction

For the reader interested in reproducing the graphics presented here, we want to present a list of the different steps taken, scripts called, and external programs used. This list is intended for users that are already somewhat familiar with TheoDORE and have worked through the tutorial that is available along with the TheoDORE distribution. All relevant input/output files of the quantum chemistry programs and TheoDORE as well as LaTeX/TikZ source files for the final graphics are available via a separate repository[86] and we urge the interested reader to download these files. Starting with $ZMSO_2M$-14TPA, first a Turbomole computation was performed. Subsequently, input for TheoDORE was generated via the `theoinp` tool. The main analysis procedure was initiated through `analyze_tden.py`, which generated individual Molden files for the NTOs as well as computing the Ω-matrices. The NTOs were plotted via the script `jmol_MOs.py`, which generates input for the Jmol program. The output was also processed via the script `plot_Om_bars.py` to produce the bar graphs shown in Fig. 2 (b-c) in the form of a LaTeX/TikZ source file. The analysis of $[Ir(ptz)_2bpy]^+$ proceeded in close analogy to $ZMSO_2M$-14TPA with the exception that the main analysis steps were already carried out using an integrated implementation[8] in Q-Chem meaning that TheoDORE was only required for the post-processing tasks. Furthermore, the dedicated analysis routines for transition metal complexes[42,43] were used in this case.

The analysis of $(FQ)_3F$ was started via `theoinp` and `analyze_tden.py` in analogy to the previous cases. The Ω-plots in Fig. 4 were subsequently produced using the `plot_OmFrag.py` functionality. The conditional densities were evaluated as cube files via the orbkit[72] interface. These were post-processed via the `vmd_plots.py` script to generate input for VMD,[75] which was subsequently used to generate the graphics in an automated fashion. The isovalues were chosen as to encompass 75% of the respective charge distribution, which proceeds via a numerical integration in `vmd_plots.py`.

V. CONCLUSIONS

We have exemplified the application of TheoDORE in three systems, an organic push-pull chromophore, a transition metal complex, and a conjugated polymer. In the first two cases, we have shown that the methods allow for an automated and quantitative analysis of excited-state character. It was seen that the fragment-based analysis is particularly useful to discern which fragments of the system contribute to the excitation and where charge transfer occurs. In the third case, we have shown that the analysis protocols provide information well beyond what could be accessed in the standard MO picture by giving detailed insight into dynamic electron-hole attraction yielding a tightly bound exciton. This was achieved via electron-hole correlation plots along with a real-space representation[27] of conditional densities and the outcomes

were interpreted in light of multiconfigurational character determined via the NTO decomposition.

The above examples served as an illustration of how TheoDORE can be used to represent the results of excited-state computations in a compact and rigorous form. Certainly, generating this data is not an end in itself but only a means to answer a scientific question. For example one can study how different substitution patterns affect the excited-state wavefunctions and correlate the results to the property of interest, e.g., singlet-triplet gaps or two-photon strengths,[41,57] and use this information in a rational design process. Alternatively, TheoDORE can be used to gain detailed insight into the dynamical behaviour of a system[49,50] or to perform statistical sampling over complex molecular systems such as DNA.[39,40]

It should not be left without saying that the fragment-based scheme also has some drawbacks. First, it is not possible to probe the shape of the orbitals, i.e., one cannot differentiate between Rydberg and valence states or between $n\pi^*$ and $\pi\pi^*$ states. Second, an a priori definition of fragments is required and the results have some dependence on the population analysis scheme chosen. To address these, we have developed an alternative analysis scheme based on multipole moments of the exciton wavefunction in real space.[10,45] These methods have been used successfully for the purpose of comparing different quantum chemistry methods,[62,87] identifying Rydberg states,[45] and to assign other elusive excited-state characteristics.[88] Nonetheless, the original TheoDORE approach, described here, remains popular considering its ease of use and lightweight nature. In the future, we hope that the fragment-based and real space approaches can both provide useful tools for practitioners in the field helping to deepen our understanding of light-driven processes in molecules.

ACKNOWLEDGMENTS

The author is grateful to L. Stojanovic, G. Hermann, S. Mai, M. F. S. J. Menger, and P. Kimber for contributing various pieces of code and acknowledges, among others, H. Lischka, I. Burghardt, A. Dreuw, S. A. Mewes, A. I. Krylov, L. González, and T. Etienne for various discussions about excited-state computations and their analysis. The author thanks P. I. P. Elliott and T. Rosenau for discussions about $[Ir(ptz)_2bpy]^+$ and $(FC)_3F$, respectively. The author extends special thanks to Theodore R. Plasser for lending his name to the project. The author gratefully acknowledges the use of the 'Lovelace' High Performance System at Loughborough University.

[1] A. V. Titov, I. S. Ufimtsev, N. Luehr, and T. J. Martinez, "Generating Efficient Quantum Chemistry Codes for Novel Architectures," J. Chem. Theory Comput. **9**, 213–221 (2013).

[2] A. I. Krylov and P. M. Gill, "Q-Chem: an engine for innovation," Wiley Interdiscip. Rev. Comput. Mol. Sci. **3**, 317–326 (2013).

[3] M. Vacher, I. Fdez. Galván, B.-W. Ding, S. Schramm, R. Berraud-Pache, P. Naumov, N. Ferré, Y.-J. Liu, I. Navizet, D. Roca-Sanjuán, W. J. Baader, and R. Lindh, "Chemi- and Bioluminescence of Cyclic Peroxides," Chem. Rev. **118**, 6927–6974 (2018).

[4] S. Ghosh, P. Verma, C. J. Cramer, L. Gagliardi, and D. G. Truhlar, "Combining Wave Function Methods with Density Functional Theory for Excited States," Chem. Rev. **118**, 7249–7292 (2018).

[5] H. Lischka, D. Nachtigallová, A. J. A. Aquino, P. Szalay, F. Plasser, F. B. C. Machado, and M. Barbatti, "Multireference approaches for excited states of molecules," Chem. Rev. **118**, 7293–7361 (2018).

[6] M. Head-Gordon, A. M. Grana, D. Maurice, and C. A. White, "Analysis of Electronic Transitions as the Difference of Electron Attachment and Detachment Densities," J. Chem. Phys. **99**, 14261–14270 (1995).

[7] R. L. Martin, "Natural transition orbitals," J. Chem. Phys. **118**, 4775–4777 (2003).

[8] F. Plasser, M. Wormit, and A. Dreuw, "New tools for the systematic analysis and visualization of electronic excitations. I. Formalism." J. Chem. Phys. **141**, 024106 (2014).

[9] M. J. G. Peach, P. Benfield, T. Helgaker, and D. J. Tozer, "Excitation energies in density functional theory: An evaluation and a diagnostic test," J. Chem. Phys. **128**, 44118 (2008).

[10] S. A. Bäppler, F. Plasser, M. Wormit, and A. Dreuw, "Exciton analysis of many-body wave functions: Bridging the gap between the quasiparticle and molecular orbital pictures," Phys. Rev. A **90**, 052521 (2014).

[11] E. Ronca, C. Angeli, L. Belpassi, F. D. Angelis, F. Tarantelli, and M. Pastore, "Density Relaxation in Time-Dependent Density Functional Theory : Combining Relaxed Density Natural Orbitals and Multireference Perturbation Theories for an Improved Description of Excited States," J. Chem. Theory Comput. **10**, 4014–4024 (2014).

[12] T. Etienne, X. Assfeld, and A. Monari, "New insight into the topology of excited states through detachment/attachment density matrices-based centroids of charge," J. Chem. Theory Comput. **10**, 3906–3914 (2014).

[13] C. Adamo, T. Le Bahers, M. Savarese, L. Wilbraham, G. Garcia, R. Fukuda, M. Ehara, N. Rega, and I. Ciofini, "Exploring excited states using Time Dependent Density Functional Theory and density-based indexes," Coord. Chem. Rev. **304-305**, 166–178 (2015).

[14] J. Coe and M. Paterson, "Characterising a configuration interaction excited state using natural transition geminals," Mol. Phys. **112**, 733–739 (2014).

[15] S. Matsika, X. Feng, A. V. Luzanov, and A. I. Krylov, "What We Can Learn from the Norms of One-Particle Density Matrices, and What We Can't: Some Results for Interstate Properties in Model Singlet Fission Systems." J. Phys. Chem. A **118**, 11943–55 (2014).

[16] G. M. J. Barca, A. T. B. Gilbert, and P. M. W. Gill, "Excitation Number: Characterizing Multiply Excited States," J. Chem. Theory Comput. **14**, 9–13 (2018).

[17] A. V. Luzanov and O. V. Prezhdo, "High-order entropy measures and spin-free quantum entanglement for molecular problems," Mol. Phys. **105**, 2879–2891 (2007).

[18] K. Boguslawski, P. Tecmer, O. Legeza, and M. Reiher, "Entanglement Measures for Single- and Multireference Correlation Effects," J. Phys. Chem. Lett. **3**, 3129–3135 (2012).

[19] F. Plasser, "Entanglement entropy of electronic excitations," J. Chem. Phys. **144**, 194107 (2016).

[20] C. J. Stein and M. Reiher, "Measuring multi-configurational character by orbital entanglement," Mol. Phys. **115**, 2110–2119 (2017), 1609.02617.

[21] E. Zojer, P. Buchacher, F. Wudl, J. Cornil, J. P. Calbert, J. L. Brédas, and G. Leising, "Excited state localization in organic molecules consisting of conjugated and nonconjugated segments," J. Chem. Phys. **113**, 10002–10012 (2000).

[22] J. Rissler, H. Bässler, F. Gebhard, and P. Schwerdtfeger, "Excited states of ladder-type poly-p-phenylene oligomers," Phys. Rev. B **64**, 045122 (2001).

[23] S. Tretiak and S. Mukamel, "Density matrix analysis and simulation of electronic excitations in conjugated and aggregated molecules," Chem. Rev. **102**, 3171–3212 (2002).

[24] J. Cornil, I. Gueli, A. Dkhissi, J. C. Sancho-Garcia, E. Hennebicq, J. P. Calbert, V. Lemaur, D. Beljonne, and J. L. Brédas, "Electronic and optical properties of polyfluorene and fluorene-based copolymers: A quantum-chemical characterization," J. Chem. Phys. **118**, 6615–6623 (2003).

[25] F. Plasser and H. Lischka, "Analysis of Excitonic and Charge Transfer Interactions from Quantum Chemical Calculations," J. Chem. Theory Comput. **8**, 2777–2789 (2012).

[26] Y. Li and C. A. Ullrich, "The Particle-Hole Map: A Computational Tool to Visualize Electronic Excitations," J. Chem. Theory Comput. **11**, 5838–5852 (2015).

[27] F. Plasser, "Visualisation of Electronic Excited-State Correlation in Real

Space," ChemPhotoChem **3**, 702–706 (2019).
[28]F. Plasser, (2019), THEODORE: a package for theoretical density, orbital relaxation, and exciton analysis; available from http://theodore-qc.sourceforge.net.
[29]H. Lischka, R. Shepard, I. Shavitt, R. M. Pitzer, M. Dallos, T. Muller, P. G. Szalay, F. B. Brown, R. Ahlrichs, H. J. Boehm, A. Chang, D. C. Comeau, R. Gdanitz, H. Dachsel, C. Ehrhardt, M. Ernzerhof, P. Hoechtl, S. Irle, G. Kedziora, T. Kovar, V. Parasuk, M. J. M. Pepper, P. Scharf, H. Schiffer, M. Schindler, M. Schueler, M. Seth, E. A. Stahlberg, J.-G. Zhao, S. Yabushita, Z. Zhang, M. Barbatti, S. Matsika, M. Schuurmann, D. R. Yarkony, S. R. Brozell, E. V. Beck, J.-P. Blaudeau, M. Ruckenbauer, B. Sellner, F. Plasser, R. F. K. Szymczak, J. J. Spada, and A. Das, "Columbus: An ab initio electronic structure program, release 7.0," www.univie.ac.at/columbus (2017).
[30]I. Fdez. Galván, M. Vacher, A. Alavi, C. Angeli, F. Aquilante, J. Autschbach, J. J. Bao, S. I. Bokarev, N. A. Bogdanov, R. K. Carlson, L. F. Chibotaru, J. Creutzberg, N. Dattani, M. G. Delcey, S. S. Dong, A. Dreuw, L. Freitag, L. M. Frutos, L. Gagliardi, F. Gendron, A. Giussani, L. González, G. Grell, M. Guo, C. E. Hoyer, M. Johansson, S. Keller, S. Knecht, G. Kovačević, E. Källman, G. Li Manni, M. Lundberg, Y. Ma, S. Mai, J. P. Malhado, P. Å. Malmqvist, P. Marquetand, S. A. Mewes, J. Norell, M. Olivucci, M. Oppel, Q. M. Phung, K. Pierloot, F. Plasser, M. Reiher, A. M. Sand, I. Schapiro, P. Sharma, C. J. Stein, L. K. Sørensen, D. G. Truhlar, M. Ugandi, L. Ungur, A. Valentini, S. Vancoillie, V. Veryazov, O. Weser, T. A. Wesołowski, P.-O. Widmark, S. Wouters, A. Zech, J. P. Zobel, and R. Lindh, "OpenMolcas: From Source Code to Insight," J. Chem. Theory Comput. **15**, 5925–5964 (2019).
[31]Y. Shao, Z. Gan, E. Epifanovsky, A. T. Gilbert, M. Wormit, J. Kussmann, A. W. Lange, A. Behn, J. Deng, X. Feng, D. Ghosh, M. Goldey, P. R. Horn, L. D. Jacobson, I. Kaliman, R. Z. Khaliullin, T. Kus, A. Landau, J. Liu, E. I. Proynov, Y. M. Rhee, R. M. Richard, M. A. Rohrdanz, R. P. Steele, E. J. Sundstrom, H. L. Woodcock, P. M. Zimmerman, D. Zuev, B. Albrecht, E. Alguire, B. Austin, G. J. Beran, Y. A. Bernard, E. Berquist, K. Brandhorst, K. B. Bravaya, S. T. Brown, D. Casanova, C. M. Chang, Y. Chen, S. H. Chien, K. D. Closser, D. L. Crittenden, M. Diedenhofen, R. A. Distasio, H. Do, A. D. Dutoi, R. G. Edgar, S. Fatehi, L. Fusti-Molnar, A. Ghysels, A. Golubeva-Zadorozhnaya, J. Gomes, M. W. Hanson-Heine, P. H. Harbach, A. W. Hauser, E. G. Hohenstein, Z. C. Holden, T. C. Jagau, H. Ji, B. Kaduk, K. Khistyaev, J. Kim, J. Kim, R. A. King, P. Klunzinger, D. Kosenkov, T. Kowalczyk, C. M. Krauter, K. U. Lao, A. D. Laurent, K. V. Lawler, S. V. Levchenko, C. Y. Lin, F. Liu, E. Livshits, R. C. Lochan, A. Luenser, P. Manohar, S. F. Manzer, S. P. Mao, N. Mardirossian, A. V. Marenich, S. A. Maurer, N. J. Mayhall, E. Neuscamman, C. M. Oana, R. Olivares-Amaya, D. P. Oneill, J. A. Parkhill, T. M. Perrine, R. Peverati, A. Prociuk, D. R. Rehn, E. Rosta, N. J. Russ, S. M. Sharada, S. Sharma, D. W. Small, A. Sodt, T. Stein, D. Stück, Y. C. Su, A. J. Thom, T. Tsuchimochi, V. Vanovschi, L. Vogt, O. Vydrov, T. Wang, M. A. Watson, J. Wenzel, A. White, C. F. Williams, J. Yang, S. Yeganeh, S. R. Yost, Z. Q. You, I. Y. Zhang, X. Zhang, Y. Zhao, B. R. Brooks, G. K. Chan, D. M. Chipman, C. J. Cramer, W. A. Goddard, M. S. Gordon, W. J. Hehre, A. Klamt, H. F. Schaefer, M. W. Schmidt, C. D. Sherrill, D. G. Truhlar, A. Warshel, X. Xu, A. Aspuru-Guzik, R. Baer, A. T. Bell, N. A. Besley, J. D. Chai, A. Dreuw, B. D. Dunietz, T. R. Furlani, S. R. Gwaltney, C. P. Hsu, Y. Jung, J. Kong, D. S. Lambrecht, W. Liang, C. Ochsenfeld, V. A. Rassolov, L. V. Slipchenko, J. E. Subotnik, T. Van Voorhis, J. M. Herbert, A. I. Krylov, P. M. Gill, and M. Head-Gordon, "Advances in molecular quantum chemistry contained in the Q-Chem 4 program package," Mol. Phys. **113**, 184–215 (2015).
[32]G. te Velde, F. M. Bickelhaupt, E. J. Baerends, C. Fonseca Guerra, S. J. A. van Gisbergen, J. G. Snijders, and T. Ziegler, "Chemistry with adf," J. Comput. Chem. **22**, 931–967 (2001).
[33]B. Aradi, B. Hourahine, and T. Frauenheim, "DFTB+, a Sparse Matrix-Based Implementation of the DFTB Method," J. Phys. Chem. A **111**, 5678–5684 (2007).
[34]A. A. Granovsky, "Firefly version 8," (2017).
[35]M. J. Frisch, G. W. Trucks, H. B. Schlegel, G. E. Scuseria, M. A. Robb, J. R. Cheeseman, G. Scalmani, V. Barone, G. A. Petersson, H. Nakatsuji, X. Li, M. Caricato, A. V. Marenich, J. Bloino, B. G. Janesko, R. Gomperts, B. Mennucci, H. P. Hratchian, J. V. Ortiz, A. F. Izmaylov, J. L. Sonnenberg, D. Williams-Young, F. Ding, F. Lipparini, F. Egidi, J. Goings, B. Peng, A. Petrone, T. Henderson, D. Ranasinghe, V. G. Zakrzewski, J. Gao, N. Rega, G. Zheng, W. Liang, M. Hada, M. Ehara, K. Toyota, R. Fukuda, J. Hasegawa, M. Ishida, T. Nakajima, Y. Honda, O. Kitao, H. Nakai, T. Vreven, K. Throssell, J. A. Montgomery, Jr., J. E. Peralta, F. Ogliaro, M. J. Bearpark, J. J. Heyd, E. N. Brothers, K. N. Kudin, V. N. Staroverov, T. A. Keith, R. Kobayashi, J. Normand, K. Raghavachari, A. P. Rendell, J. C. Burant, S. S. Iyengar, J. Tomasi, M. Cossi, J. M. Millam, M. Klene, C. Adamo, R. Cammi, J. W. Ochterski, R. L. Martin, K. Morokuma, O. Farkas, J. B. Foresman, and D. J. Fox, "Gaussian~16 Revision C.01," (2016), gaussian Inc. Wallingford CT.
[36]F. Neese, "Software update: the ORCA program system, version 4.0," Wiley Interdiscip. Rev. Comput. Mol. Sci. **8**, e1327 (2018).
[37]I. S. Ufimtsev and T. J. Martinez, "Quantum chemistry on graphical processing units. 1. strategies for two-electron integral evaluation," J. Chem. Theory Comput. **4**, 222–231 (2008).
[38]TURBOMOLE V7.2 2017, a development of University of Karlsruhe and Forschungszentrum Karlsruhe GmbH, 1989-2007, TURBOMOLE GmbH, since 2007; available from http://www.turbomole.com.
[39]F. Plasser, A. J. A. Aquino, W. L. Hase, and H. Lischka, "UV Absorption Spectrum of Alternating DNA Duplexes. Analysis of Excitonic and Charge Transfer Interactions," J. Phys. Chem. A **116**, 11151–11160 (2012).
[40]J. J. Nogueira, F. Plasser, and L. González, "Electronic delocalization, charge transfer and hypochromism in the UV absorption spectrum of polyadenine unravelled by multiscale computations and quantitative wavefunction analysis," Chem. Sci. **8**, 5682–5691 (2017).
[41]F. Glöcklhofer, A. Rosspeintner, P. Pasitsuparoad, S. Eder, J. Fröhlich, G. Angulo, E. Vauthey, and F. Plasser, "Effect of symmetric and asymmetric substitution on the optoelectronic properties of 9,10-dicyanoanthracene," Mol. Syst. Des. Eng. **4**, 951–961 (2019).
[42]F. Plasser and A. Dreuw, "High-Level Ab Initio Computations of the Absorption Spectra of Organic Iridium Complexes," J. Phys. Chem. A **119**, 1023–1026 (2015).
[43]S. Mai, F. Plasser, J. Dorn, M. Fumanal, C. Daniel, and L. González, "Quantitative wave function analysis for excited states of transition metal complexes," Coord. Chem. Rev. **361**, 74–97 (2018).
[44]S. A. Mewes, J.-M. Mewes, F. Plasser, and A. Dreuw, "Excitons in poly(para phenylene vinylene): A quantum-chemical perspective based on high-level ab initio calculations," Phys. Chem. Chem. Phys. **18**, 2548–2563 (2016).
[45]F. Plasser, B. Thomitzni, S. A. Bäppler, J. Wenzel, D. R. Rehn, M. Wormit, and A. Dreuw, "Statistical analysis of electronic excitation processes: Spatial location, compactness, charge transfer, and electron-hole correlation," J. Comp. Chem. **36**, 1609–1620 (2015).
[46]A. V. Luzanov and O. A. Zhikol, "Electron Invariants and Excited State Structural Analysis for Electronic Transitions Within CIS, RPA, and TDDFT Models," Int. J. Quantum Chem. **110**, 902–924 (2010).
[47]I. Mayer, "Bond order and valence: Relations to Mulliken's population analysis," Int. J. Quantum Chem. **26**, 151–154 (1984).
[48]A. A. Voityuk, "Fragment transition density method to calculate electronic coupling for excitation energy transfer." J. Chem. Phys. **140**, 244117 (2014).
[49]F. Plasser, G. Granucci, J. Pittner, M. Barbatti, M. Persico, and H. Lischka, "Surface hopping dynamics using a locally diabatic formalism: charge transfer in the ethylene dimer cation and excited state dynamics in the 2-pyridone dimer." J. Chem. Phys. **137**, 22A514 (2012).
[50]S. Mai and L. González, "Unconventional two-step spin relaxation dynamics of [Re(CO) 3 (im)(phen)] + in aqueous solution," Chem. Sci. **10**, 10405–10411 (2019).
[51]K. Hummer and C. Ambrosch-Draxl, "Oligoacene exciton binding energies: Their dependence on molecular size," Phys. Rev. B **71**, 081202 (2005).
[52]W. Aggoune, C. Cocchi, D. Nabok, K. Rezouali, M. A. Belkhir, and C. Draxl, "Dimensionality of excitons in stacked van der Waals materials: The example of hexagonal boron nitride," Phys. Rev. B **97**, 1–6 (2018).
[53]P. Bultinck, D. L. Cooper, and R. Ponec, "Influence of atoms-in-molecules methods on shared-electron distribution indices and domain-averaged fermi holes," J. Phys. Chem. A **114**, 8754–8763 (2010).
[54]J. B. Schriber, K. P. Hannon, C. Li, and F. A. Evangelista, "A Combined Selected Configuration Interaction and Many-Body Treatment of Static and Dynamical Correlation in Oligoacenes," J. Chem. Theory Comput. **14**, 6295–6305 (2018).

[55]S. A. Mewes, F. Plasser, and A. Dreuw, "Communication: Exciton analysis in time-dependent density functional theory: How functionals shape excited-state characters," J. Chem. Phys. **143**, 171101 (2015).
[56]F. Plasser, M. Wormit, S. A. Mewes, B. Thomitzni, and A. Dreuw, "LIBWFA: Wave-function analysis tool library for quantum chemical applications; available from `https://github.com/libwfa/libwfa`.".
[57]P. Kautny, F. Glöcklhofer, T. Kader, J.-M. Mewes, B. Stöger, J. Fröhlich, D. Lumpi, and F. Plasser, "Charge-transfer states in triazole linked donor–acceptor materials: strong effects of chemical modification and solvation," Phys. Chem. Chem. Phys. **19**, 18055–18067 (2017).
[58]S. I. Bokarev, O. S. Bokareva, and O. Kühn, "Electronic excitation spectrum of the photosensitizer $[ir(ppy)_2(bpy)]^+$." J. Chem. Phys. **136**, 214305 (2012).
[59]B. J. Powell, "Theories of phosphorescence in organo-transition metal complexes - From relativistic effects to simple models and design principles for organic light-emitting diodes," Coord. Chem. Rev. **295**, 46–79 (2015).
[60]B. Beyer, C. Ulbricht, D. Escudero, C. Friebe, A. Winter, L. González, and U. S. Schubert, "Phenyl-1H-[1,2,3]triazoles as new cyclometalating ligands for iridium(III) complexes," Organometallics **28**, 5478–5488 (2009).
[61]P. A. Scattergood and P. I. Elliott, "An unexpected journey from highly tunable phosphorescence to novel photochemistry of 1,2,3-triazole-based complexes," Dalt. Trans. **46**, 16343–16356 (2017).
[62]S. A. Mewes, F. Plasser, and A. Dreuw, "Universal Exciton Size in Organic Polymers is Determined by Non-Local Orbital Exchange in TDDFT," J. Phys. Chem. Lett. **8**, 1205–1210 (2017).
[63]W. Barford, "Excitons in conjugated polymers: a tale of two particles." J. Phys. Chem. A **117**, 2665–71 (2013).
[64]T. Rosenau, A. Potthast, N. S. Zwirchmayr, H. Hettegger, F. Plasser, T. Hosoya, M. Bacher, K. Krainz, and T. Dietz, "Chromophores from hexeneuronic acids: identification of HexA-derived chromophores," Cellulose **24**, 3671–3687 (2017).
[65]N. S. Zwirchmayr, T. Hosoya, H. Hettegger, M. Bacher, K. Krainz, T. Dietz, U. Henniges, A. Potthast, and T. Rosenau, "Chromophores from hexeneuronic acids: chemical behavior under peroxide bleaching conditions," Cellulose **24**, 3689–3702 (2017).
[66]A. Kumar, G. Cappellini, and F. Delogu, "Electronic and optical properties of chromophores from hexeneuronic acids," Cellulose **26**, 1489–1501 (2019).
[67]A. N. Panda, F. Plasser, A. J. A. Aquino, I. Burghardt, and H. Lischka, "Electronically excited states in poly(p-phenylenevinylene): vertical excitations and torsional potentials from high-level ab initio calculations." J. Phys. Chem. A **117**, 2181–2189 (2013).
[68]S. van der Walt, S. C. Colbert, and G. Varoquaux, "The NumPy Array: A Structure for Efficient Numerical Computation," Comput. Sci. Eng. **13**, 22–30 (2011).
[69]J. D. Hunter, "Matplotlib: A 2D Graphics Environment," Comput. Sci. Eng. **9**, 90–95 (2007).
[70]N. M. O'Boyle, M. Banck, C. A. James, C. Morley, T. Vandermeersch, and G. R. Hutchison, "Open Babel: An open chemical toolbox," J. Cheminform. **3**, 33 (2011).
[71]N. M. O'Boyle, A. L. Tenderholt, and K. M. Langner, "cclib: A library for package-independent computational chemistry algorithms," J. Comput. Chem. **29**, 839–845 (2008).
[72]G. Hermann, V. Pohl, J. C. Tremblay, B. Paulus, H. C. Hege, and A. Schild, "ORBKIT: A modular python toolbox for cross-platform postprocessing of quantum chemical wavefunction data," J. Comput. Chem. **37**, 1511–1520 (2016), 1601.03069.
[73]M. D. Hanwell, D. E. Curtis, D. C. Lonie, T. Vandermeersch, E. Zurek, and G. R. Hutchison, "Avogadro: an advanced semantic chemical editor, visualization, and analysis platform," Journal of cheminformatics **4**, 17 (2012).
[74]JMOL: an open-source Java viewer for chemical structures in 3D; available from http://www.jmol.org/.
[75]W. Humphrey, A. Dalke, and K. Schulten, "Vmd: Visual molecular dynamics," Journal of Molecular Graphics **14**, 33 – 38 (1996).
[76]Schrödinger, LLC, "The PyMOL molecular graphics system, version 1.8," (2015).
[77]F. Plasser, (2019), qc_pymol: scripts for using pymol together with quantum chemistry programs; available from https://github.com/felixplasser/qc_pymol.
[78]C. Hattig, "Structure optimizations for excited states with correlated second-order methods: CC2 and ADC(2)," Advances in Quantum Chemistry, Vol 50 **50**, 37–60 (2005).
[79]A. Schafer, H. Horn, and R. Ahlrichs, "Fully optimized contracted gaussian-basis sets for atoms li to kr," J. Chem. Phys. **97**, 2571–2577 (1992).
[80]S. Hirata and M. Head-Gordon, "Time-dependent density functional theory within the Tamm–Dancoff approximation," Chem. Phys. Lett. **314**, 291–299 (1999).
[81]C. Adamo and V. Barone, "Toward reliable density functional methods without adjustable parameters: The PBE0 model," J. Chem. Phys. **110**, 6158–6170 (1999).
[82]A. D. Becke, "Density-functional thermochemistry. iii. the role of exact exchange," J. Chem. Phys. **98**, 5648–5652 (1993).
[83]C. Lee, W. Yang, and R. G. Parr, "Development of the colle-salvetti correlation-energy formula into a functional of the electron density," Phys. Rev. B **37**, 785–789 (1988).
[84]T. Yanai, D. P. Tew, and N. C. Handy, "A new hybrid exchange-correlation functional using the coulomb-attenuating method (CAM-B3LYP)," Chem. Phys. Lett. **393**, 51–57 (2004).
[85]F. Neese, F. Wennmohs, A. Hansen, and U. Becker, "Efficient, approximate and parallel Hartree–Fock and hybrid DFT calculations. A 'chain-of-spheres' algorithm for the Hartree–Fock exchange," Chem. Phys. **356**, 98–109 (2009).
[86]Supporting research data available: Molecular geometries, input/output files of the employed quantum chemistry programs and TheoDORE; data and LaTeX/TikZ source files underlying the figures. DOI: 10.17028/rd.lboro.11382459 .
[87]S. A. Mewes, F. Plasser, A. Krylov, and A. Dreuw, "Benchmarking excited-state calculations using exciton properties," J. Chem. Theory Comput. **14**, 710–725 (2018).
[88]M. Hoffmann, S. A. Mewes, S. Wieland, C. Popp, and A. Dreuw, "Electron–Hole Correlation as Unambiguous and Universal Classification for the Nature of Low-Lying $\pi\pi^*$ States of Nitrogen Heterocycles," J. Phys. Chem. Lett. **10**, 6112–6117 (2019).